Quantitative analysis of the native presynaptic cytomatrix by cryoelectron tomography

Rubén Fernández-Busnadiego,[1] Benoît Zuber,[2] Ulrike Elisabeth Maurer,[1] Marek Cyrklaff,[1] Wolfgang Baumeister,[1] and Vladan Lučić[1]

[1]Department of Molecular Structural Biology, Max Planck Institute of Biochemistry, D-82152 Martinsried, Germany
[2]Medical Research Council Laboratory of Molecular Biology, CB2 0QH Cambridge, England, UK

The presynaptic terminal contains a complex network of filaments whose precise organization and functions are not yet understood. The cryoelectron tomography experiments reported in this study indicate that these structures play a prominent role in synaptic vesicle release. Docked synaptic vesicles did not make membrane to membrane contact with the active zone but were instead linked to it by tethers of different length. Our observations are consistent with an exocytosis model in which vesicles are first anchored by long (>5 nm) tethers that give way to multiple short tethers once vesicles enter the readily releasable pool. The formation of short tethers was inhibited by tetanus toxin, indicating that it depends on soluble *N*-ethyl-maleimide sensitive fusion protein attachment protein receptor complex assembly. Vesicles were extensively interlinked via a set of connectors that underwent profound rearrangements upon synaptic stimulation and okadaic acid treatment, suggesting a role of these connectors in synaptic vesicle mobilization and neurotransmitter release.

Introduction

Presynaptic terminals are highly specialized neuronal compartments enclosing neurotransmitter-filled synaptic vesicles and the machinery necessary for vesicle exocytosis. When a depolarizing stimulus arrives at the presynaptic terminal, Ca^{2+} influx causes vesicle fusion at a region of the presynaptic membrane directly facing the postsynaptic side, the so-called active zone (AZ), thereby releasing neurotransmitter into the synaptic cleft. Neurotransmitter diffuses across the cleft to reach the postsynaptic receptors of the partner cell, thus establishing synaptic communication.

The organization of synaptic vesicles is usually described in terms of functional pools (Rizzoli and Betz, 2005). The readily releasable pool (RRP) consists of vesicles that can be immediately exocytosed upon Ca^{2+} influx; they are primed for release and thought to be docked to the AZ. However, not all docked vesicles belong to the RRP. The recycling pool is formed by vesicles released to sustain synaptic transmission under mild stimulation and includes the RRP. Vesicles mobilized only under strong stimulation constitute the reserve pool.

Correspondence to Wolfgang Baumeister: baumeist@biochem.mpg.de

M. Cyrklaff's present address is Dept. of Parasitology, Institute of Infectious Diseases, University of Heidelberg, D-69120 Heidelberg, Germany.

Abbreviations used in this paper: AZ, active zone; HB, homogenization buffer; HBM, Hepes-buffered medium; HSV-1, Herpes simplex virus 1; HTS, hypertonic sucrose; K-W test, Kruskal-Wallis test; OA, okadaic acid; RRP, readily releasable pool; TeTx, tetanus toxin; WBP, weighted back projection.

Filamentous structures are abundant in the presynaptic terminal. However, the composition of this presynaptic cytomatrix and its role in the synaptic vesicle cycle are not well understood. Previous studies have reported the existence of filaments connecting synaptic vesicles to the AZ and short strands linking vesicles to each other or to longer filaments (Landis et al., 1988; Hirokawa et al., 1989; Gotow et al., 1991). Although these strands were hypothesized to consist of synapsin, recent electron tomographic work showed that some persisted in synapsin knockout mice, suggesting that other molecules are also involved (Siksou et al., 2007).

To investigate the precise organization of the presynaptic cytomatrix, we have performed cryoelectron tomography on vitrified frozen-hydrated, unstained synapses from the mammalian central nervous system. Electron tomography allows 3D imaging of cellular landscapes (Koster et al., 1997; Lučić et al., 2005a), whereas sample vitrification ensures optimal preservation (Dubochet et al., 1988). Because heavy metal stain is not applied, the contrast is directly related to the intrinsic density of the biological material. All previous EM studies on presynaptic

© 2010 Fernández-Busnadiego et al. This article is distributed under the terms of an Attribution–Noncommercial–Share Alike–No Mirror Sites license for the first six months after the publication date (see http://www.jcb.org/misc/terms.shtml). After six months it is available under a Creative Commons License (Attribution–Noncommercial–Share Alike 3.0 Unported license, as described at http://creativecommons.org/licenses/by-nc-sa/3.0/).

The Rockefeller University Press $30.00
J. Cell Biol. Vol. 188 No. 1 145–156
www.jcb.org/cgi/doi/10.1083/jcb.200908082

THE JOURNAL OF CELL BIOLOGY

Downloaded from http://rupress.org/jcb/article-pdf/188/1/145/1893572/jcb_200908082.pdf by guest on 08 February 2026

architecture were performed on dehydrated samples, which are known to suffer from the aggregation of cytoplasmic components and other artifacts that may affect data interpretation (Dubochet and Sartori Blanc, 2001; Al-Amoudi et al., 2004).

We studied two complementary synaptic preparations: cryosections from rat hippocampal organotypic slices and rat cerebrocortical synaptosomes. Organotypic slices provide a close approximation to nervous tissue, but their cryopreparation yields sections that suffer from cryosectioning-induced compression and whose thickness limits the volume that can be studied (Han et al., 2008). Synaptosomes are a well-established model for neurotransmitter release and are susceptible to pharmacological manipulations (Nicholls and Sihra, 1986; Harrison et al., 1988).

Synaptosomes were subjected to pharmacological treatments aimed at either causing synaptic vesicle release or modulating it. Exocytosis was induced by (a) the application of hypertonic sucrose (HTS) leading to the release of the RRP (Rosenmund and Stevens, 1996) and (b) high concentrations of KCl, mobilizing both the RRP and the reserve pool (Ashton and Ushkaryov, 2005; Rizzoli and Betz, 2005). Neurotransmitter release was modulated by (a) incubation with tetanus toxin (TeTx), a clostridial neurotoxin that prevents SNARE complex formation and synaptic vesicle fusion by cleaving the vesicular SNARE protein synaptobrevin/vesicle-associated membrane protein (Schiavo et al., 2000), and (b) the phosphatase inhibitor okadaic acid (OA), which alters the phosphorylation state of synapsin (Jovanovic et al., 2001) and increases vesicle mobility (Betz and Henkel, 1994) and neurotransmitter release (Sim et al., 1993).

The tomographic datasets were analyzed by means of a novel segmentation algorithm that incorporated previous work (Lučić et al., 2005b) into the framework of the watershed segmentation. Using a segmentation mask in which the AZ and the synaptic vesicles were manually traced, this procedure allowed the automated detection and analysis of the filamentous structures linked to the AZ or vesicles (see Materials and methods). The combination of pharmacological manipulations, cryoelectron tomography, and automated data analysis allowed us to study the presynaptic cytomatrix in its native state and gain structural insights into its role in synaptic vesicle organization and release.

Results

Morphology of frozen-hydrated presynaptic terminals

We recorded and analyzed 33 tomograms of cryopreserved presynaptic terminals from untreated rat cerebrocortical synaptosomes, synaptosomes subjected to different pharmacological treatments, and rat hippocampal organotypic slices (Table S1).

As expected for samples preserved in vitreous ice, membranes had a smooth and continuous appearance without signs of aggregation and deposition of the cytoplasmic material (Fig. 1). Presynaptic terminals had diameters from 0.4 to 1 µm (enclosing volumes from 0.03 to 0.3 μm^3), typically hosting 100–500 synaptic vesicles (Fig. 1, A [synaptosomes] and C [organotypic slices]; note that in cryosections of organotypic slices, synaptic vesicles are compressed in the cutting direction). The AZ had a typical length of 200–400 nm. The terminals often contained mitochondria and occasionally cytoskeletal elements such as microtubules or actin, which are consistent in appearance with those observed in other preparations (Garvalov et al., 2006; Medalia et al., 2007). Interestingly, OA treatment induced the formation of bundles of long (>100 nm) actin filaments generally observed further than 300 nm from the AZ and oriented nearly parallel to it (Fig. 1 B). Actin filaments were often seen in postsynaptic terminals (Fig. 1 D).

The vitrification of organotypic slices required the use of cryoprotective agents, resulting in increased osmolarity (additional ∼300 mOsm) and reversible effects on the physiological properties of the slice (Zuber et al., 2005). Synaptic morphology in slices was compared with synaptosomes under different hypertonic solutions (100 mM and 300 mM HTS) to account for the higher resistance of nervous tissue to hypertonicity compared with synaptosomes (Ashton and Ushkaryov, 2005). In agreement with that study, all synaptosomes treated with 300 mM HTS showed major morphological perturbations with many endosomal or vacuolar compartments, elongated synaptic vesicles, and lacking vesicles close to the AZ (unpublished data). Synaptosomes treated with 100 mM HTS were visually indistinguishable from untreated synaptosomes and organotypic slices (apart from the cryosectioning-induced compression). Given that the preparation procedure of synaptosomes and organotypic slices are entirely different (unlike slices, synaptosomes are detached from cells and may lose some cytosolic components but are kept under isotonic conditions), it is unlikely that they introduce similar artifacts. Therefore, when compared with 100 mM HTS-treated synaptosomes, slices can serve at least as a partial control for alterations induced by synaptosomal preparation. In addition, the hypertonic treatment used for the subsequent analysis (100 mM HTS for 60 s) was previously shown to cause an exclusive and complete release of the RRP in synaptosomes (Ashton and Ushkaryov, 2005).

The viability of synaptosomes was confirmed by glutamate release assay (Fig. S1; Nicholls and Sihra, 1986; Godino et al., 2007). None of the treatments resulted in morphological changes indicative of damage, confirming synaptosome integrity. In fact, all of these treatments have been extensively characterized in synaptosomes by previous studies. Specifically, the incubation of synaptosomes with 30 mM KCl was shown to induce massive neurotransmitter release over several minutes (Nicholls and Sihra, 1986), whereas higher KCl concentrations did not cause additional release (Marks and McMahon, 1998). Also, the treatment of synaptosomes with 200 nM TeTx for 2 h is consistent with the conditions shown to induce cleavage of synaptobrevin (McMahon et al., 1992; Ashton and Dolly, 2000). Synaptosomes have been incubated over several minutes with micromolar concentrations of OA to alter the phosphorylation state of several synaptic proteins in a variety of studies (Sim et al., 1993; Vaughan et al., 1997; Lonart et al., 2003). At the concentration used in this study (1 µM for 15 min), OA completely inhibits the activity of both protein phosphatases 1 and 2A (Cohen et al., 1990).

In both synaptosomes and organotypic slices, numerous filamentous structures were present on the membrane of the synaptic vesicles, which is in agreement with the reported high density of membrane proteins (Südhof, 2004). Most vesicles

Downloaded from http://rupress.org/jcb/article-pdf/188/1/145/1893572/jcb_200908082.pdf by guest on 08 February 2026

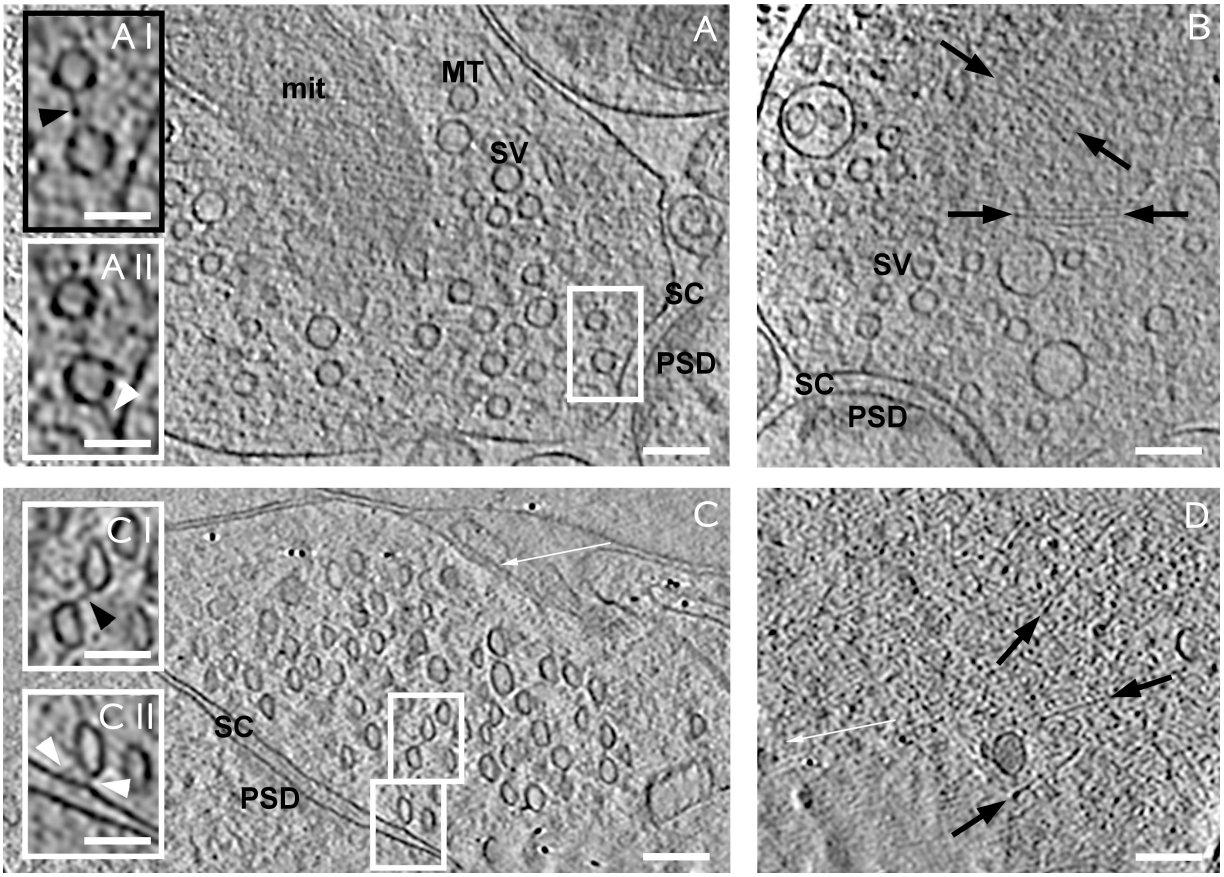

Figure 1. **Presynaptic morphology visualized in tomograms of frozen-hydrated synapses.** (A) Untreated synaptosome. (A, I) Connector linking two vesicles (black arrowhead). (A, II) Tether linking a vesicle to the AZ (white arrowhead; same vesicles as in A [I] at another z slice). (B) OA-treated synaptosome showing presynaptic actin bundles (black arrows). (C) Organotypic slice. Synaptic vesicles are compressed along the cutting direction (white arrows in C and D). (C, I) Connector linking two vesicles (black arrowhead). (C, II) Tethers linking a vesicle to the AZ (white arrowheads). (D) Postsynaptic terminal showing actin filaments (black arrows). Tomographic slices are 2.7-nm thick. Insets show magnified views of boxed areas. SV, synaptic vesicle; mit, mitochondrion; MT, microtubule; SC, synaptic cleft; PSD, postsynaptic density. Bars: (main panels) 100 nm; (insets) 50 nm.

were linked to at least one neighbor by short filaments up to 40-nm long (termed connectors; Fig. 1, A [I] and C [I]). Many vesicles were linked to the AZ by short filaments (tethers; Fig. 1, A [II] and C [II]). Direct contact between cellular and vesicular membranes was observed only in a few cases (see Direct membrane contact between….). For the subsequent analysis, connectors and tethers were automatically segmented (Fig. 2).

Inhomogeneity in the spatial distribution of synaptic vesicles

We assessed presynaptic vesicle distribution by measuring the fraction of cytoplasmic volume occupied by vesicles for the first 250 nm from the AZ (Fig. 2 A). In every untreated synaptosome, synaptic vesicle concentration had a maximum close to the AZ and a minimum at a distance of 50–70 nm to it ($P < 0.05$ between minima and maxima by paired *t* test; Fig. 3 A). The mean ratio between minima and maxima was 0.38 ± 0.18. Further away from the AZ, vesicle concentration increased again. Similar results were obtained for individual synapses in organotypic slices and HTS-treated synaptosomes, whereas vesicle distribution was clearly altered for KCl- and OA-treated synaptosomes. In these cases, vesicle concentration was lowest near the AZ and increased with distance.

To facilitate quantitative data analysis, we divided the presynaptic terminal into four zones, according to the distribution of vesicles in untreated synaptosomes: proximal (0–45 nm from the AZ, where the maximum of vesicle density was located), intermediate (45–75 nm, containing the density minimum), and two distal zones of similar thickness further away from the AZ (first, 75–150 nm; second, 150–250 nm). Taking all untreated synaptosomes together, synaptic vesicle concentration in the intermediate zone was significantly lower than in the proximal and distal zones ($P < 0.05$ and $P < 0.01$, respectively, by *t* test; Fig. 3 C). In organotypic slices, each individual synapse showed an intermediate region of reduced vesicle concentration (Fig. 3 A). However, the location of this region was different in every synapse because not all sections were perpendicular to the cleft and because of the sectioning-induced compression. Thus, the region of reduced vesicle concentration was not evident upon averaging (Fig. 3 C).

In KCl-treated synaptosomes, the overall vesicle concentration and the concentration in the proximal and second distal zones were significantly reduced compared with untreated synaptosomes ($P < 0.05$ and $P < 0.01$ and $P < 0.05$ by *t* test; Fig. 3, B and C, respectively). The concentration profile of OA-treated synaptosomes (Fig. 3) was similar to that of the KCl-stimulated

Downloaded from http://rupress.org/jcb/article-pdf/188/1/145/1893572/jcb_200908082.pdf by guest on 08 February 2026

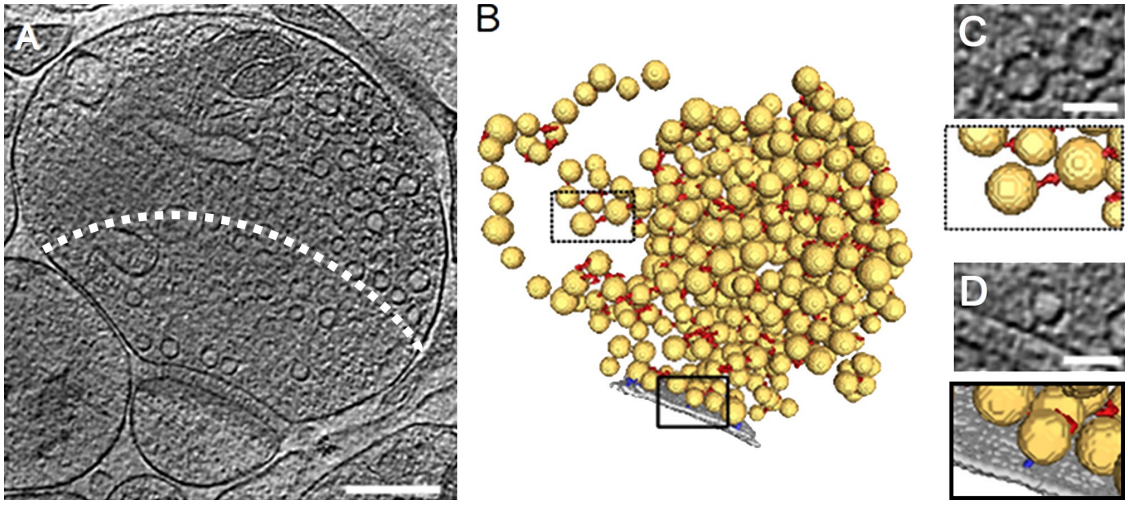

Figure 2. **Segmentation procedure.** (A) 2.7-nm-thick tomographic slice of a 100-mM HTS-treated synaptosome. The dashed line indicates the analyzed area (first 250 nm from the AZ). (B) 3D segmentation of synaptic vesicles (yellow), AZ (gray), synaptic vesicle connectors (red), and synaptic vesicle tethers (blue). Boxed regions are magnified in C and D. (C and D, top) Tomographic slices showing a synaptic vesicle connector (C) and a tether (D) and their 3D visualization as detected by the automated segmentation procedure (bottom). Bars: (A) 200 nm; (C and D) 50 nm.

case. Thus, our data provides detailed structural evidence for the stimulating effect of OA, which was previously detected using biochemical methods (Sim et al., 1993).

Extensive interconnectivity of synaptic vesicles

The analysis of the interaction between synaptic vesicles and connectors gave very similar results for untreated, HTS-treated synaptosomes, and organotypic slices. More than 80% of the vesicles were linked to one or more of their neighbors via synaptic vesicle connectors (Fig. 4 A). For untreated synaptosomes, this fraction did not change significantly with increasing distance from the AZ (Fig. 4 B), despite the significant variation of vesicle concentration (Fig. 3 C). The number of connectors per vesicle was slightly higher in the distal zones of untreated synaptosomes ($P < 0.05$ in both cases by Kruskal-Wallis test [K-W test]; Fig. 4 C) and did not differ significantly from HTS-treated synaptosomes and organotypic slices. About half of the connected vesicles had more than two connectors (Fig. S2 A).

The fraction of connected vesicles (Fig. 4, A [whole terminal] and B [proximal zone]) and the number of connectors per connected vesicle in the distal zones (Fig. 4 C) were significantly reduced in KCl-stimulated synaptosomes compared with untreated ones ($P < 0.001$ by χ^2 and K-W tests, respectively). OA-treated synaptosomes gave very similar results, except that in the proximal zone, the fraction of connected vesicles did not differ significantly from untreated synaptosomes (Fig. 4 B). In TeTx-treated synaptosomes, connectivity was reduced only in the proximal zone ($P < 0.001$ by χ^2 test; Fig. 4 B).

We estimated the length of the connectors by measuring the distance between their contact points with vesicles (see Materials and methods; Fig. 4 D). Connector length was only slightly higher than the (minimal) distance between connected vesicles, indicating that the connectors were very close to spanning the shortest path between vesicles. Almost all connectors were shorter than 40 nm, and in untreated synaptosomes, 87% were shorter than 20 nm (Fig. S2 B). Nevertheless, some of the longer connectors might have been missed because of noise. We did not analyze connector length for organotypic slices because it might have been affected by cryosectioning-induced compression.

The mean connector length in untreated synaptosomes was significantly reduced in the proximal zone ($P < 0.01$ by K-W test; Fig. 4 E). OA treatment reduced connector length in the proximal and intermediate zones ($P < 0.01$ and $P < 0.05$, respectively, by K-W test) but increased the length in both distal zones ($P < 0.001$ by K-W test). Taken together with the nonnormal distribution of connector lengths (Fig. S2 B), these results suggest that more than one type of connectors is present and that OA has a differential effect on them.

Clusters of interconnected synaptic vesicles

We defined a cluster of interconnected vesicles as a group of vesicles all linked to each other via connectors. These clusters can be defined precisely and may underlie the closely packed groups of vesicles traditionally observed in EM. Thus, the study of such clusters reveals the influence of connectivity in vesicle distribution.

Typically, a presynaptic terminal contained >20 clusters of interconnected vesicles. Cluster size varied considerably, ranging from two vesicle clusters to large clusters of >50 vesicles. These large clusters dominated in untreated synaptosomes, comprising 61% of the connected vesicles (51% of all vesicles; Fig. S3 A). Fig. S3 D shows a visualization of the clusters of interconnected vesicles in an untreated synaptosome.

Under KCl stimulation, large clusters were absent (Fig. S3 A), and the size of the largest cluster relative to the total number of vesicles in each terminal was reduced ($P < 0.01$ by K-W test; Fig. S3 B). OA-treated synaptosomes showed an intermediate situation (Fig. S3 A), with the size of the largest cluster reduced compared with untreated ones ($P < 0.01$ by K-W test; Fig. S3 B).

Downloaded from http://rupress.org/jcb/article-pdf/188/1/145/1893572/jcb_200908082.pdf by guest on 08 February 2026

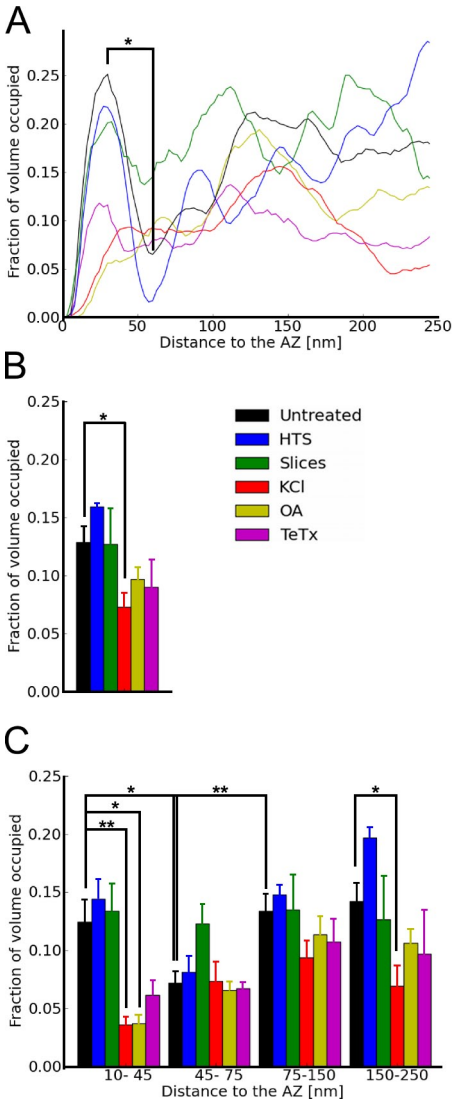

Figure 3. **Synaptic vesicle distribution within presynaptic terminals depicted as the fraction of cytoplasmic volume occupied by vesicles.** (A) Representative traces of individual synapses. (B) Vesicle concentration for the first 250 nm from the AZ. (C) Vesicle concentration versus distance to the AZ. Plots show mean values and SEM (error bars). The confidence values are indicated by * and ** for $P < 0.05$ and $P < 0.01$, respectively. The number of presynaptic terminals analyzed for each treatment is shown in Table S1.

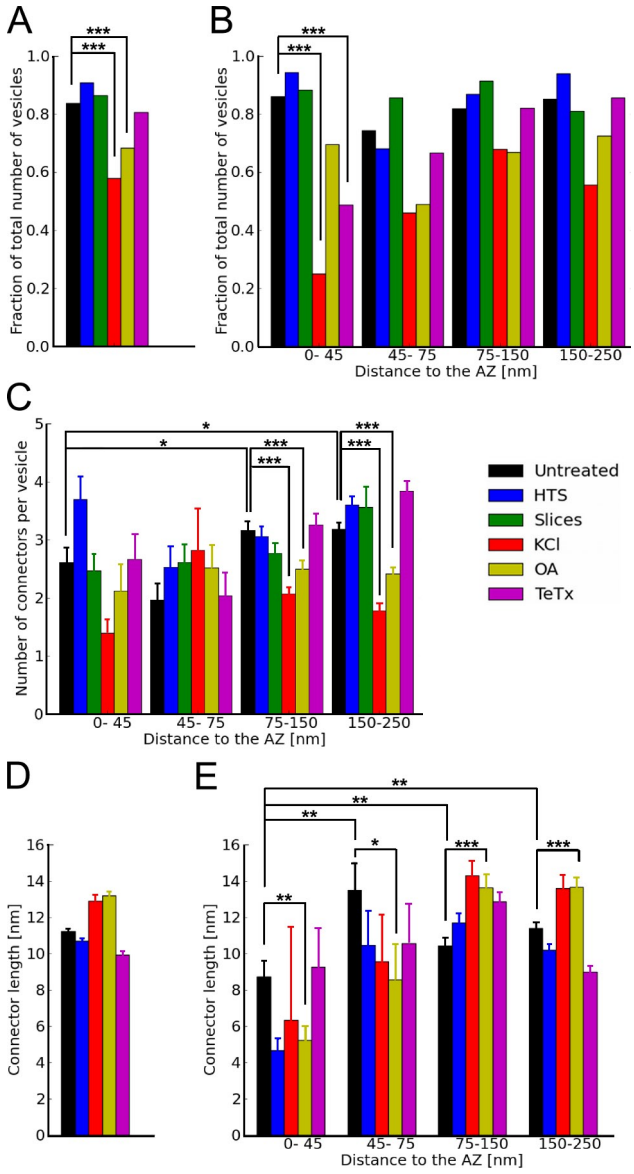

Figure 4. **Synaptic vesicle connectors.** (A) Fraction of connected vesicles for the first 250 nm from the AZ. (B) Fraction of connected vesicles versus distance to the AZ. (C) Number of connectors per connected vesicle versus distance to the AZ. (D) Connector length for the first 250 nm from the AZ. (E) Connector length versus distance to the AZ. Plots show mean values and SEM (error bars). The confidence values are indicated by *, **, and *** for $P < 0.05$, $P < 0.01$, and $P < 0.001$, respectively. The numbers of vesicles (A and B) and connectors (C–E) analyzed for each treatment are shown in Table S1.

Clusters of interconnected vesicles extended considerably in the direction perpendicular to the AZ. In five out of seven untreated synapses, at least one cluster spanned from the proximal to the distal zone. In contrast, this was observed only in one out of six synapses treated with KCl. Vesicles in distal zones belonged to larger clusters than those in the proximal and intermediate zones ($P < 0.001$ by K-W test; untreated synaptosomes; Fig. S3 C). Compared with untreated synaptosomes, cluster size was reduced for KCl- and OA-stimulated synapses both in the proximal ($P < 0.01$ by K-W test) and distal zones ($P < 0.001$), but clusters in OA-treated synaptosomes were still significantly larger than under KCl in the distal zones ($P < 0.001$). Note that spatial distribution of cluster sizes (Fig. S3 C) differed from that of vesicles (Fig. 3) and vesicle connectivity (Fig. 4 B). All in all, synaptic vesicle clusters were significantly disrupted by KCl and to a lower extent by OA, even though both treatments caused a similar vesicle mobilization (Fig. 3 C).

Tethering of proximal synaptic vesicles to the AZ

Filaments of variable length (Fig. 5 and Fig. 6 C) tethered the majority of the synaptic vesicles in the proximal zone to the AZ in untreated, HTS, TeTx-treated synaptosomes, and organotypic slices, whereas tethering was significantly reduced for KCl and OA treatments ($P < 0.001$ by χ^2 test; Fig. 6 A). All tethered

Downloaded from http://rupress.org/jcb/article-pdf/188/1/145/1893572/jcb_200908082.pdf by guest on 08 February 2026

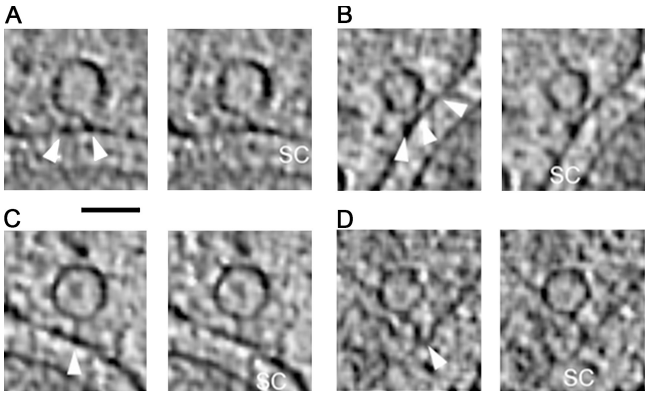

Figure 5. **Images of synaptic vesicle tethers.** (A–D) Short (A and B; <5 nm) and long (C and D; >5 nm) synaptic vesicle tethers (white arrowheads) are shown. SC, synaptic cleft. Two consecutive 2.7-nm-thick tomographic slices are shown for each case. Bar, 50 nm.

vesicles were located in the proximal zone, and only rarely was there a direct contact between vesicle and cell membranes. Compared with untreated synapses, there was a significantly lower number of tethers per vesicle in the HTS-treated case ($P < 0.001$ by K-W test; Fig. 6 B), which is largely the result of the low number of vesicles having more than two tethers ($P < 0.01$ by χ^2 test; Fig. S2 C).

HTS, TeTx, and OA-treated synapses had a reduced number of short tethers (<5 nm; Fig. S2 D) that resulted in an increase of the mean tether length ($P < 0.001$ by K-W test; Fig. 6 C). Thus, under hypertonic conditions and TeTx treatment, tethered vesicles were held to the membrane by fewer tethers, and this reduction was mainly caused by the loss of the short tethers. Images of short (Fig. 5, A and B) and long (Fig. 5, C and D) tethers are presented in Fig. 5.

Conversely, when vesicles with more than two tethers were excluded from untreated synapses, the number of tethers per vesicle and the mean tether length were indistinguishable from HTS- or TeTx-treated synaptosomes (Fig. 6, B and C). Therefore, our results showed that (a) vesicles released by HTS, i.e., those that form the RRP (Ashton and Ushkaryov, 2005), had a larger number of short tethers (more than two per vesicle under our experimental conditions), and (b) TeTx prevented the formation of short tethers.

We also investigated the relationship between tethering to the AZ and vesicle connectivity. When vesicles were separated in categories according to their tethering and connectivity states, untreated and HTS-treated synaptosomes and organotypic slices showed a similar pattern (Fig. 6 D). Interestingly, tethers were significantly shorter for connected vesicles in untreated synaptosomes ($P < 0.001$ by K-W test; Fig. S2 E), whereas tethering had no effect on connector length. Also, many tethered vesicles belonged to clusters of interconnected vesicles that reached the distal zones (21 of 60 tethered vesicles in four out of seven untreated synapses), indicating a potential cross talk between tethered and distal vesicles.

Tethers and other electron-dense structures emanating from the AZ that did not contact vesicles did not form regular patterns. Also, the positions of proximal vesicles and both types of densities were not correlated (Fig. S2 F).

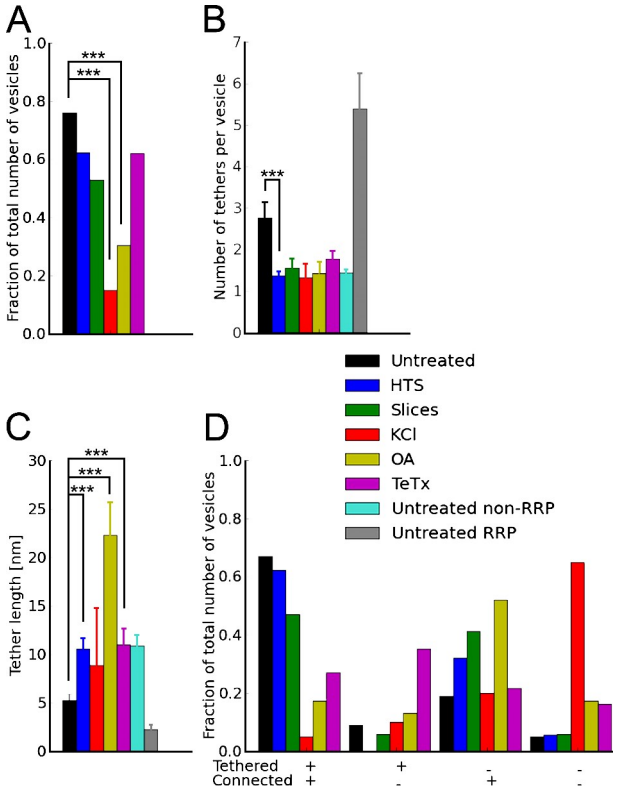

Figure 6. **Synaptic vesicle tethers.** (A) Fraction of proximal synaptic vesicles tethered to the AZ. (B) Mean number of tethers per tethered synaptic vesicle. Untreated RRP and untreated non-RRP: tethered vesicles with more than two and up to two tethers in untreated synaptosomes, respectively. (C) Tether length for all tethered vesicles. (D) Fraction of proximal synaptic vesicles as a function of tethering and connectivity. Plots show mean values and SEM (error bars). The confidence values are indicated by *** for $P < 0.001$. The numbers of vesicles (A, B, and D) and tethers (C) analyzed for each treatment are shown in Table S1.

Synaptic vesicle size

Synaptic vesicle diameter in untreated synaptosomes was 41.6 ± 5.6 nm (mean ± SD), and the distribution of diameters could be fitted by a Gaussian curve (Fig. S4 A). In untreated synaptosomes, vesicle diameter was slightly larger in the proximal zone than in all others ($P < 0.05$ by *t* test; Fig. S4 B).

Synaptic vesicle diameter was significantly reduced for OA- and TeTx-treated synaptosomes ($P < 0.001$ by *t* test; $\Delta V = -20\%$ and $\Delta V = -17\%$, respectively). This was not caused by a difference in synapse type because most of the analyzed synapses were excitatory (five out of six OA-treated, all TeTx-treated, and six out of seven untreated synapses presented a strong postsynaptic density).

In the proximal zone, the tethering and connectivity states of synaptic vesicles influenced vesicle diameter in untreated, HTS-, and KCl-treated synaptosomes (Fig. S4 C). In untreated synaptosomes, tethered (connected) vesicles were larger than nontethered (nonconnected) ones. In particular, tethered and connected vesicles were much larger those nontethered and nonconnected ($P < 0.01$ by *t* test; $\Delta V = +100\%$; Fig. S4 C). Considering the first 250 nm from the AZ, connected vesicles were only larger in OA-treated synapses ($P < 0.01$ by *t* test; $\Delta V = +11\%$; unpublished data). As vesicles were significantly compressed in

Downloaded from http://rupress.org/jcb/article-pdf/188/1/145/1893572/jcb_200908082.pdf by guest on 08 February 2026

slices, their diameter was not measured. A semiquantitative representation summarizing the values for vesicle size, connectivity, and tethering for the different groups of samples is shown in Fig. S4 D. We did not observe any correlation between tethering or connectivity and the electron density of the vesicle lumen.

Direct membrane contact between synaptic vesicles and the AZ

In our synaptic preparations, direct membrane to membrane contact between synaptic vesicles and the AZ was rarely observed and only found in tomograms of untreated synaptosomes. However, these contacts appeared to be more common in tomograms of synaptosomes inoculated with Herpes simplex virus 1 (HSV-1; Maurer et al., 2008), which were included in this analysis. Vesicles associated with the AZ were captured either with an open pore ($n = 2$; Fig. 7 A) or making contact with an invagination of the AZ ($n = 4$; Fig. 7 B). We also observed patches of AZ of unusually high, concave curvature ($n = 2$; Fig. 7 C), likely signatures of full-collapse fusion events. These snapshots (Fig. 7) correspond well to the recently proposed steps of synaptic vesicle fusion (Fig. 2 in Martens and McMahon, 2008).

Each of the two vesicles observed with an open pore at the AZ retained an almost spherical shape, forming a cylindrical neck of ~19 nm in length and 14 nm outer diameter that contained an aqueous channel with a diameter of ~3 nm. Interestingly, both vesicles were connected to their neighbors and showed no signs of clathrin coating.

A prominent L-shaped density was detected close to the AZ invagination for three out of four vesicles making membrane contact with the AZ (Fig. 7 B, arrowhead). The density consisted of two arms, one shorter (~14 nm), contacting the vesicle, and one longer (~17 nm), contacting the AZ. The arms formed angles between 100 and 140°, showing higher density at their junction. Remarkably, a similar L-shaped density was observed on the side of the necks for vesicles with an open pore (Fig. 7 A), but in this case, the arm contacting the AZ was considerably fainter than the vesicular arm. Thus, such density was detected in five out of six examples of vesicles directly associated with the cell membrane. In contrast, it was not observed in any of 15 randomly chosen tethered vesicles, indicating that the formation of the L-shaped density was preferentially correlated with the direct membrane contact between vesicles and the AZ ($P < 0.001$ by K-W test).

Discussion

Combining cryoelectron tomography with pharmacological manipulations, we provided a quantitative assessment of the structural elements mediating synaptic vesicle organization and release in mammalian central nervous system synapses. The rearrangement of the short connectors interlinking synaptic vesicles upon synaptic stimulation and inhibition of phosphatases suggests that these connectors play an important role in vesicle mobilization. Furthermore, the comparison between synapses at rest and those stimulated by KCl or HTS points to a link between the configuration of the tethering assembly and vesicle availability

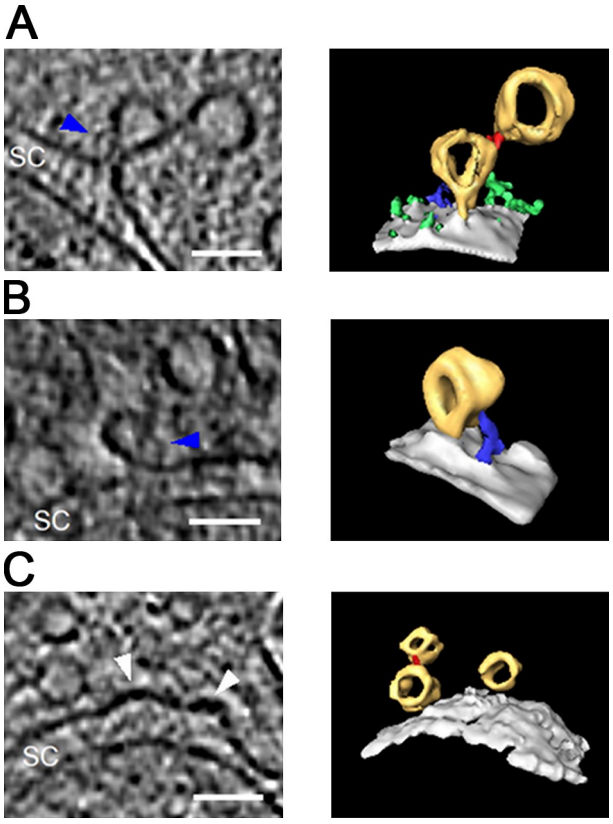

Figure 7. **Direct membrane contact between synaptic vesicles and the AZ.** (A–C, left) 2.7-nm-thick tomographic slices and the corresponding direct 3D rendering of the EM densities (right) are shown. (A) Synaptic vesicle with an open neck, which establishes continuity between the vesicular lumen and the extracellular space. An L-shaped density is visible close to the neck (blue arrowhead). (B) Synaptic vesicle making membrane contact with an invagination of the AZ. An L-shaped density is present close to the AZ invagination (blue arrowhead). (C) Regions of the AZ with high concave curvature (white arrowheads), which are likely signatures of full-collapse fusion events. Yellow, synaptic vesicles; red, synaptic vesicle connectors; gray, AZ; blue, synaptic vesicle–associated densities; green, other AZ densities. SC, synaptic cleft. Bars, 50 nm.

for release. Connectors and tethers were the most prominent components of the presynaptic cytomatrix, and longer filaments were rarely observed.

3D analysis of vitrified presynaptic terminals

By means of sample vitrification, artifacts arising from chemical fixation, dehydration, and staining were avoided. Furthermore, the use of an automated procedure for segmentation of connectors and tethers and for data analysis allowed a comprehensive and quantitative description of the most prominent presynaptic features. The validity of the segmentation procedure was confirmed by (a) the good correspondence between the structures observed in tomograms by visual inspection with those segmented automatically (Fig. 2) and (b) the fact that the distance between vesicles (in the case of connectors) or vesicles and AZ (tethers) was not determinant for the detection of either kind of filaments, as shown by the pharmacological effects on the abundance, distribution, and morphology of connectors (Fig. 4, B and E) and tethers (Fig. 6, A and C) that cannot be explained simply

Downloaded from http://rupress.org/jcb/article-pdf/188/1/145/1893572/jcb_200908082.pdf by guest on 08 February 2026

by changes in vesicle distribution (Fig. 3 C). However, because of the limited tilt range and high level of noise inherent to cryo-electron tomograms (Lučić et al., 2005a), it is possible that the numbers of connectors and tethers may have been underestimated by the segmentation procedure.

The analysis of vesicle distribution and connectivity for untreated synaptosomes, HTS-treated synaptosomes (under conditions corresponding to the increased osmolarity necessary for slice vitrification), and organotypic slices gave very similar results (Fig. 3 A; and Fig. 4, A and B). When an effect of hypertonicity was detected, such as a reduced number of tethers, it was comparable in HTS-treated synaptosomes and organotypic slices (Fig. 6). Furthermore, synaptosomes showed functional neurotransmitter release in glutamate release assays (Fig. S1). Thus, our data strongly suggest that cryopreserved synaptosomes complemented by cryosections of organotypic brain slices form a suitable experimental system for investigating both presynaptic architecture and vesicle release.

The role of synaptic vesicle connectors in vesicle mobilization

Previous EM studies observed abundant filaments of different lengths in presynaptic terminals at rest, suggesting an important role of these structures in synaptic function. It was proposed that in resting synapses, vesicles were linked to each other and/or to the cytoskeleton via short strands, which would be released upon synaptic activity to allow vesicle mobilization (Rizzoli and Betz, 2005). However, no experimental evidence for such proposal was presented so far, and the molecular identity of such strands remains uncertain. Although an early study identified these short filaments with synapsin (Hirokawa et al., 1989), recent work showed that some of them persisted in synapsin triple knockout mice, indicating that other molecules must also be implicated in their formation (Siksou et al., 2007).

Our analysis showed that in resting synapses, short connectors (<40 nm) linked >80% of vesicles to their neighbors, forming interconnected vesicle clusters of various size, ranging from few to >50 vesicles (Fig. 4 A and Fig. S3 A). Synaptic stimulation with KCl resulted in an overall reduction in synaptic vesicle concentration and connectivity and a major disruption of vesicle clusters. A similar effect was observed under OA treatment, arguing that the removal of connectors is a morphological correlate of the OA-induced dispersion of vesicles (Betz and Henkel, 1994) and increase in vesicle mobility (Kraszewski et al., 1996). Considering the absence of any other major structural elements in vitrified frozen-hydrated presynaptic terminals, we conclude that (a) synaptic vesicle clustering is mainly mediated by short connectors that link vesicles to each other rather than to a cytoskeletal matrix and that (b) the connectors are dynamic structures, and treatments known to increase vesicle mobility, such as KCl stimulation or OA-mediated elevation in phosphorylation levels, cause the removal of the connectors. In fact, the dynamic binding and unbinding of vesicles to each other via connectors may provide a mechanistic basis for the stick and diffuse model (Shtrahman et al., 2005). Therefore, our data suggest that the connectors play a dual role, limiting vesicle dispersion in resting synapses and regulating vesicle mobilization for neurotransmitter release during synaptic activity.

Our results (Fig. 4 E and Fig. S2 B) suggest that there is more than one molecular species of connectors and indicate that OA has a differential effect on them. Alternatively, our data could be explained by multiple OA-dependent conformational states of one connector type, regulated by differentially localized factors. In any case, the decrease in the connectivity of proximal (but not distal) vesicles under TeTx (Fig. 4 B) implicates synaptobrevin in the formation of connectors in the proximal zone.

Our data also provide an explanation for the observed transition of the OA effect on neurotransmitter release from facilitatory to inhibitory as a function of incubation time (Koss et al., 2007). After a 15-min incubation with 1 µM OA, bundles of long filaments, likely to consist on actin, were visually identified growing parallel to the AZ (Fig. 1 B). Although OA might initially facilitate neurotransmitter release by partial removal of vesicle connectors, after longer incubation, filamentous bundles growing parallel to the AZ would hinder mobilization of distant vesicles toward the AZ, resulting in net inhibition of release.

Differences in diameter between connected and nonconnected vesicles were only minor for all treatments except OA, in which connected vesicles were larger, suggesting that a target of OA is involved in the regulation of vesicle size.

AZ organization, tethering, and synaptic vesicle progression toward fusion

At the ultrastructural level, the exact organization of the AZ remains controversial because of the disparity of results obtained using different EM sample preparation procedures. Thus, in chemically fixed, heavy metal–stained samples, docked vesicles were reported to accumulate around regularly arranged pyramidal densities (Phillips et al., 2001). In studies using high pressure freezing followed by freeze substitution and staining, docked vesicles also clustered around electron-dense material on the AZ, but such structures did not form any regular pattern (Siksou et al., 2007). Numerous filaments but not focal densities were observed at the AZ in cryofixed, unstained, freeze-fractured samples (Landis et al., 1988). More recently, AZ filaments were also observed using freeze substitution (Siksou et al., 2009b). Our tomograms of vitrified, frozen-hydrated synapses revealed that even though the AZ was rich in small densities, these densities were not arranged regularly, and they did not cluster vesicles in their proximities (Fig. S2 F).

Different studies also present conflicting views on the way that vesicles proximal to the AZ associate or dock to it. When chemical fixation and staining were used, docked vesicles were often reported to make direct membrane contact with the AZ or to even be hemifused with it (Zampighi et al., 2006). However, these results need to be interpreted carefully. First, fixatives introduce cross-linking artifacts and may alter the distribution of vesicles within the presynaptic terminal (Siksou et al., 2009a). Second, the biological structures are not observed directly but are surrounded by a layer of stain of a certain thickness.

Thus, even though synaptic vesicle tethering to the AZ has been postulated to be a necessary step before docking, priming, and fusion (Gerber et al., 2008; Verhage and Sørensen, 2008), the tethering and docking machinery have been elusive to EM methods based on chemical fixation (Schweizer and Ryan, 2006;

Downloaded from http://rupress.org/jcb/article-pdf/188/1/145/1893572/jcb_200908082.pdf by guest on 08 February 2026

Verhage and Sørensen, 2008). In cryofixed, dehydrated samples, direct membrane contact between vesicles and AZ (but not hemifusion) was reported, as well as tethering filaments of variable length (Siksou et al., 2007, 2009b). In our tomograms of unstained, fully hydrated specimens, membrane contact occurred only during vesicle fusion or fission. Most of the proximal vesicles of untreated synapses were tethered to the AZ by filaments shorter than 40 nm. Therefore, our results strongly suggest that the tethers are the main mechanism of synaptic vesicle association to the AZ and argue against hemifusion as a stable intermediate.

The RRP is functionally well characterized, but its morphological definition is still debated (Rosenmund and Stevens, 1996; Schweizer and Ryan, 2006; Verhage and Sørensen, 2008). In synaptosomes, incubation with 100 mM HTS for 60 s is known to cause the complete and exclusive release of the RRP (Ashton and Ushkaryov, 2005). Our data showed that synaptosomes under this hypertonic solution were distinguished from untreated ones by a reduced number of vesicles with more than two short tethers (<5 nm). This indicates that vesicles with more than two short tethers constitute the RRP (Fig. 6 B and Fig. S2 C). Therefore, our results suggest that both the number and nature of the tethers are indicative of synaptic vesicle progression toward fusion.

Different types of tethers were present as indicated by their wide range of lengths (Fig. S2 D). Furthermore, the quantitative analysis of mean number of tethers per vesicle and mean tether length (Fig. 6, B and C) yielded remarkably similar values for TeTx- and HTS-treated synaptosomes. Although longer tethers (>5 nm) remained unaffected, short tethers were significantly reduced by TeTx action compared with the untreated case. This strongly suggests that TeTx prevents formation of the short tethers, most probably by synaptobrevin cleavage and subsequent abolishment of SNARE complex assembly. Our results cannot clarify whether the fully assembled SNARE complex constitutes the short tethers, but this hypothesis would be consistent with the notion that (primed) synaptic vesicles are located within 3–4 nm from the AZ upon SNARE complex formation (Martens and McMahon, 2008).

These results also support the lack of SNARE complex involvement in the formation of the longer tethers, as reported for other tethering systems (Sztul and Lupashin, 2006). In fact, SNARE-independent tethers of similar shape bind cargo vesicles to the endoplasmic reticulum (Tripathi et al., 2009), whereas tethering in mammalian synapses has been proposed to be mediated by the tripartite complex formed by Munc13, RIM, and Rab3 (Dulubova et al., 2005). Nevertheless, the dimensions of the longer tethers suggest that they could mediate the stabilization of vesicles ~20 nm away from the cell membrane described in total internal reflection fluorescence studies (Zenisek et al., 2000; Karatekin et al., 2008), necessary for SNARE complex assembly (Parpura and Mohideen, 2008). Finally, the drastic reduction of tethering observed during prolonged KCl stimulation could be a consequence of the recently proposed AZ disruption after exocytosis (Hosoi et al., 2009; Wu et al., 2009).

Our observations suggest the following structural model of synaptic vesicle exocytosis: (a) initially, long, SNARE-independent filaments tether the vesicles to the AZ, (b) long tethers give way to multiple shorter ones in a SNARE-dependent transition that makes the vesicle available for immediate release, and (c) upon establishment of membrane to membrane contact, exocytosis takes place. A similar model was recently proposed for the ER to Golgi vesicle traffic in which transport vesicles are first tethered to the Golgi membrane by long, SNARE-independent factors and are then brought into an ~50-Å distance from the membrane to allow SNARE assembly and subsequent fusion (Kim et al., 2006).

In untreated synapses, proximal synaptic vesicles were larger than distal ones (Fig. S4 B). Furthermore, in the proximal zone, tethered and/or connected vesicles were larger than nontethered, nonconnected vesicles (Fig. S4 C). Considering the involvement of tethering in vesicle release, one may speculate that the increase in size is correlated with vesicle progression toward exocytosis. Alternatively, different molecular compositions may determine vesicle size (Wojcik et al., 2004) and the exact sequence of steps leading to release (Verhage and Sørensen, 2008).

Six cases of direct membrane contact between a vesicle and the AZ were imaged (Fig. 7, A and B). The increased frequency of these events in synaptosomes incubated with HSV-1 could be caused by an elevation of cytoplasmic Ca^{2+} concentration upon interaction of the virus with the cellular membrane (Zhou et al., 2009). Because the association of the virus with the presynaptic membrane can take place at any point over an extended incubation period, it may be easier to detect exo/endocytic events upon freezing than 1 min after KCl stimulation. In two cases, a well-defined, cylindrical neck was observed establishing continuity between the vesicular lumen and the extracellular space. These vesicles were located at the AZ and not coated, making it unlikely that they represent clathrin-mediated endocytosis. They may instead correspond to fusion events or, alternatively, to clathrin-independent endocytosis (such as in kiss and run mechanism), as suggested by their elongated necks. The direct membrane contact between vesicles and AZ was strongly correlated with the appearance of L-shaped densities consisting of two arms, one contacting the vesicle and the other one the cell membrane, reminiscent to those observed by Zampighi et al., (2006). Because of their large size, it is unlikely that they correspond to assembled SNARE complexes. Additionally, each of the vesicles observed with an open pore was connected to a neighbor, indicating that the connectors may play an active role during exo/endocytosis.

Synaptic vesicle distribution in resting synapses is not homogenous

Synaptic vesicle distribution in untreated terminals was characterized by similar vesicle concentrations in the proximal and distal zones with a reduction in the intermediate region (45–75 nm away from the AZ; Fig. 3, A and C). A comparable distribution was observed in HTS-treated synaptosomes and individual synapses in organotypic slices. Nevertheless, this effect was averaged out in organotypic slices by sectioning artifacts. KCl application resulted in a significant loss of vesicles in the whole terminal, more pronounced close to the AZ, as observed in other synaptic preparations (Janka and Jones, 1982).

Downloaded from http://rupress.org/jcb/article-pdf/188/1/145/1893572/jcb_200908082.pdf by guest on 08 February 2026

The very low abundance of presynaptic cytoskeletal elements may seem hard to reconcile with current views on the role of actin in presynaptic terminals, as well as with the nonuniform vesicle distribution reported in this study. However, because monomeric actin, transient, or very short actin filaments that do not interlink vesicles could not be detected by our segmentation procedure, our results do not preclude the involvement of actin in processes such as scaffolding of regulatory molecules (Sankaranarayanan et al., 2003) or vesicle endocytosis (Bourne et al., 2006). However, we showed that a great majority of vesicles in the whole terminal are connected to each other, whereas in the proximal zone, they are both interconnected and tethered to the AZ. Thus, the lower vesicle concentration in the intermediate zone could be generated by the opposing dynamics of the AZ, attracting vesicles to the proximal zone via the tethering mechanism and the large clusters of interconnected vesicles dominating the distal zones. Furthermore, the mobilization of distal vesicles toward the AZ could be mediated by the interplay between tethering and connectivity, as indicated by clusters that reached from tethered vesicles to the distal zones, complemented with the free diffusion of nonconnected vesicles (or those forming smaller clusters) through the intermediate zone.

Materials and methods

Synaptosomal preparation

Cerebrocortical synaptosomes were extracted from 6–8-wk-old male Wistar rats as described previously (Dunkley et al., 1988; Godino et al., 2007) in accordance with the procedures accepted by the Max Planck Institute for Biochemistry. In brief, anesthetized animals were decapitated, and the cortex was extracted and homogenized in homogenization buffer (HB; 0.32 M sucrose, 50 mM EDTA, 20 mM DTT, and one tablet of Complete mini EDTA-free protease inhibitor cocktail [Roche]/10 ml, pH 7.4) with up to seven strokes at 700 rpm in a Teflon glass homogenizer. The homogenate was centrifuged for 2 min at 2,000 *g*, and the pellet was resuspended in HB and centrifuged for another 2 min at 2,000 *g*. Supernatants from both centrifugations were combined and centrifuged for 12 min at 9,500 *g*. The pellet was resuspended in HB and loaded onto a three-step Percoll gradient (3%, 10%, and 23%; Sigma-Aldrich) in HB without protease inhibitor cocktail. The gradients were spun for 6 min at 25,000 *g*, and the material accumulated at the 10/23% interface was recovered and diluted to a final volume of 100 ml in Hepes-buffered medium (HBM; 140 mM NaCl, 5 mM KCl, 5 mM $NaHCO_3$, 1.2 mM Na_2HPO_4, 1 mM $MgCl_2$, 10 mM glucose, and 10 mM Hepes, pH 7.4). Percoll was removed by an additional washing step with HBM by centrifugation for 10 min at 22,000 *g*, and the pellet was resuspended in HBM and immediately used in the experiments. All steps were performed at 4°C.

Glutamate release assay

This assay measures the ability of synaptosomes to release glutamate by synaptic vesicle exocytosis as a response to an external depolarization of the membrane (Nicholls and Sihra, 1986; Godino et al., 2007). A synaptosomal solution of 1 mg/ml in HBM was supplemented with 1 mg/ml BSA and incubated for 1 h at 37°C. 1.33 mM $CaCl_2$, 1 mM $NADP^+$, and 50 U/ml of glutamate dehydrogenase were added, and the increase in fluorescence as a result of the reduction of $NADP^+$ upon addition of 30 mM KCl was measured at excitation and emission wavelengths of 340 nm and 460 nm, respectively (LS50 spectrometer; PerkinElmer). The curves were calibrated by the addition of 4 nmol glutamate. Control experiments to determine the nonexocytic component of glutamate release were performed in the absence of Ca^{2+}.

Pharmacological treatments and vitrification of synaptosomes

Synaptosomes were diluted to ∼1 mg/ml protein concentration determined by Bradford assay (Bio-Rad Laboratories), preincubated for 1 h at 37°C, and vitrified. Pharmacological treatments were applied before vitrification by incubating synaptosomes for (a) 1 min with 30 mM KCl, (b) 1 min with 100 or 300 mM HTS (synaptosomes in 300 mM HTS were not analyzed), (c) 2 h with 200 nM TeTx (Merck), omitting the 1-h preincubation, or (d) 15 min with 1 µM OA (Merck). Additionally, synaptosomes inoculated with HSV-1 strain wild-type 17 (Maurer et al., 2008) for 60 min on ice and for 2, 30, or 60 min at room temperature were included in the synaptic vesicle fusion experiment.

For vitrification, a 3-µl drop of 10-nm colloidal gold (Sigma-Aldrich) was deposited on plasma-cleaned, holey carbon copper EM grids (Quantifoil) and allowed to dry. A 3-µl drop of synaptosomal suspension was placed onto the grid, blotted with filter paper (GE Healthcare), and plunged into liquid ethane. Vitrified grids were either transferred directly to the microscope cryoholder or stored in liquid nitrogen.

Hippocampal slice cultures, high pressure freezing, and cryosectioning

Transverse 400-µm-thick hippocampal slices were prepared from 6–7-d-old Wistar rats and maintained for 10–15 d in culture as described previously (Stoppini et al., 1991). They were high pressure frozen after a 5-min immersion in medium supplemented with 20% dextran (40 kD) and 5% sucrose as described previously (Zuber et al., 2005).

Thin sections (50–80-nm feed) were obtained as described previously (Zuber et al., 2005) with a cryo-ultramicrotome (UC6/FC6; Leica) and a 35° cryoimmuno–diamond knife (Diatome). Sections were transferred onto 400 × 100 mesh grids (Agar Scientific) coated with a thin layer of carbon. Subsequently, fiducial markers (PbSe Core EviDots; Evident Technologies) were applied on the sections as described previously (Masich et al., 2006).

Cryoelectron tomography

Tilt series were collected under a low dose acquisition scheme (Koster et al., 1997) using microscopes (CM300 [Philips] and T30 Polara [FEI]) operated at 300 kV. Both microscopes were equipped with a field emission gun, a 2k × 2k charge-coupled device camera (Gatan), a post-GIF energy filter (Gatan) operated in the zero-loss mode, and a computerized cryostage designed to maintain the specimen temperature <−150°C. Tilt series were typically recorded from −60° to 60° with a 2° angular increment. Pixel sizes were 0.68 (CM300) and 0.66 nm (Polara) at the specimen level, and the defocus was set to −9 µm. The total dose was kept <80 $e^-/Å^2$.

Tilt series were aligned using gold beads as fiducial markers, and 3D reconstructions were obtained by weighted back projection (WBP) using the TOM toolbox (Nickell et al., 2005). During reconstruction, the projections were binned twice (final voxel size of 2.72 and 2.64 nm) and low pass filtered at the post-binning Nyquist frequency. The resolution of the tomograms was limited by the voxel size. The tomograms were subsequently denoised by anisotropic nonlinear diffusion (Fernández and Li, 2003). The simultaneous iterative reconstruction technique was used in some cases (see Data analysis).

Image segmentation

The AZ was manually segmented in Amira (TGS). In synaptosomes, a maximum-diameter profile (along z axis) was manually traced for each vesicle, which was then segmented by substituting it with a sphere of the same diameter and center using a custom-made routine. The comparison with vesicles segmented by manual tracing of all profiles confirmed that spheres provided a good approximation for vesicles as described previously (Harris and Sultan, 1995). Vesicles in cryosections were segmented by tracing all profiles because they were elongated as a result of cutting-induced deformations. The outer membrane diameter of vesicles was measured, and only those with a diameter of 20–60 nm were considered as synaptic vesicles and included in the analysis.

A comprehensive and objective segmentation and analysis of molecular complexes that connect membranes at the presynaptic terminal were implemented as a combination of watershed transformation (Soille, 2003) and thresholding and connectivity segmentation (Lučić et al., 2005b). In short, the presynaptic cytoplasm of each tomogram was segmented using the watershed segmentation, which included a wide range of thresholds. Only those segments that contacted exactly two vesicles (connectors) or one vesicle and the AZ (tethers) were retained (Fig. 2) because other segment types were not found by visual inspection. The thresholds used for the segmentation ranged from the lowest grayscale values of a tomogram to the mean grayscale value. The exact threshold values had negligible influence on the segmentation, as most of the segments were detected at intermediate thresholds. Thus, difficulties associated with uneven background levels as well as the choice of a particular threshold were avoided.

To minimize the influence of the missing wedge, tomograms of synapses with different orientations of their AZs in respect to the tilt axis were recorded. The number of detected tethers showed only a weak and statistically insignificant dependence on the AZ orientation.

Downloaded from http://rupress.org/jcb/article-pdf/188/1/145/1893572/jcb_200908082.pdf by guest on 08 February 2026

Data analysis

The morphological properties, location parameters, and grayscale values were determined for all synaptic vesicles, tethers, and connectors of each synapse separately. For the analysis of vesicle distribution (Fig. 3), the part of the interior of the presynaptic terminal occupied by synaptic vesicles was divided into 1-pixel-thick layers according to the distance to the AZ, and the fraction of layer volume occupied by vesicles was measured. Possible bias as a result of differences in size among individual synapses was thereby avoided. In all other cases involving vesicle distance to the AZ (Figs. 4, 6, S3 and S4), the distance of the vesicle center to the AZ was used. All parameters, except those related to vesicle clusters, were analyzed only in the first 250 nm from the AZ, as vesicles in this region are the main candidates to participate in exocytosis during relatively short stimulations. For cluster analysis, the whole presynaptic terminals were considered. The numbers of analyzed tomograms, synaptic vesicles, connectors, and tethers are summarized in Table S1.

Connector and tether lengths were estimated based on the positions of contact voxels in which the contact voxels of a connector are those that contact the vesicle membranes (those that contact the vesicle membrane and the AZ in the case of tethers). To take curvature into account, the length was calculated as the sum of straight-line distances between (centers of) contact voxels and a middle voxel (a voxel belonging to the connector/tether that is equidistant from the two membranes). A more intuitive estimate of connector/tether lengths would be to measure the lengths from edge to edge. However, this is well defined only for straight connectors/tethers, in which case edge to edge lengths are one voxel size ($\sim$2.7 nm) longer than estimates presented in this study. For example, a straight linear connector reported to have length of 5.4 nm is composed of three voxels (because distance between centers of the first and the third voxel is two voxel sizes) and would have an edge to edge length of 8.1 nm.

Filaments from the AZ that did not contact vesicles were segmented in the same way as the tethers, but they were only required to contact the AZ. The colocalization of proximal synaptic vesicles and densities on the AZ was assessed by the correlation between vesicle locations and electron density of the cytoplasm in the first 8 nm from the AZ.

For the analysis of connectivity, clustering, tethering, and vesicle size and distribution, values calculated for each treatment were combined and statistically analyzed to generate the results shown in Figs. 3, 4, 6, S2 (A–E), S3, and S4. Means were calculated over all measurements of a specific property. For example, the fraction of volume occupied by vesicles was averaged over synapses and connector length over connectors. We used a Student's *t* test for statistical analysis of values that appeared to be normally distributed (e.g., vesicle diameter) and the K-W test (nonparametric) for values deviating from the normal distribution (e.g., number of tethers/connectors per vesicle). When values fell into discrete bins (e.g., fraction of connected and nonconnected vesicles), the χ^2 test was used. In all cases, confidence levels were calculated using two-tailed tests. The confidence values were indicated in the graphs by *, $P < 0.05$; **, $P < 0.01$; and ***, $P < 0.001$.

Electron density of vesicle lumen was calculated in tomograms reconstructed by WBP as well as by simultaneous iterative reconstruction technique, an algorithm that represents low spatial frequencies with higher fidelity than WBP. In both cases, the lumenal density was normalized in respect to the vesicle membrane density.

The segmentation and analysis software was written in Python programming language using the numerical and scientific packages NumPy and SciPy (http://www.scipy.org). It was executed under Linux on Opteron-based architecture, with a typical single processor run time for one synapse of several hours.

Online supplemental material

Fig. S1 shows the results of the glutamate release assay, demonstrating functional neurotransmitter release in synaptosomes. Fig. S2 shows the analysis of the number of connectors and tethers per synaptic vesicle, analysis of connector and tether length, and a stereo view of the AZ from the cytoplasmic side. Fig. S3 shows the analysis and visualization of synaptic vesicle clusters. Fig. S4 shows the analysis of synaptic vesicle size. Table S1 provides the number of experiments, tomograms, synaptic vesicles, connectors, and tethers analyzed for each group of samples. Online supplemental material is available at http://www.jcb.org/cgi/content/full/jcb.200908082/DC1.

We would like to thank Drs. Gabriela J. Greif and Eri Sakata for critical reading of the manuscript and Drs. María del Carmen Godino and José Sánchez-Prieto for sharing with us their expertise in synaptosome preparation.

This work was supported by a Deutsche Forschungsgemeinschaft grant (SPP 1288). B. Zuber is supported by a European Molecular Biology Organization long-term fellowship and thanks Nigel Unwin for his support.

Submitted: 17 August 2009
Accepted: 4 December 2009

References

Al-Amoudi, A., L.P.O. Norlen, and J. Dubochet. 2004. Cryo-electron microscopy of vitreous sections of native biological cells and tissues. *J. Struct. Biol.* 148:131–135. doi:10.1016/j.jsb.2004.03.010

Ashton, A.C., and J.O. Dolly. 2000. A late phase of exocytosis from synaptosomes induced by elevated $[Ca^{2+}]i$ is not blocked by clostridial neurotoxins. *J. Neurochem.* 74:1979–1988. doi:10.1046/j.1471-4159.2000.0741979.x

Ashton, A.C., and Y.A. Ushkaryov. 2005. Properties of synaptic vesicle pools in mature central nerve terminals. *J. Biol. Chem.* 280:37278–37288. doi:10.1074/jbc.M504137200

Betz, W.J., and A.W. Henkel. 1994. Okadaic acid disrupts clusters of synaptic vesicles in frog motor nerve terminals. *J. Cell Biol.* 124:843–854. doi:10.1083/jcb.124.5.843

Bourne, J., J.R. Morgan, and V.A. Pieribone. 2006. Actin polymerization regulates clathrin coat maturation during early stages of synaptic vesicle recycling at lamprey synapses. *J. Comp. Neurol.* 497:600–609. doi:10.1002/cne.21006

Cohen, P., C.F.B. Holmes, and Y. Tsukitani. 1990. Okadaic acid: a new probe for the study of cellular regulation. *Trends Biochem. Sci.* 15:98–102. doi:10.1016/0968-0004(90)90192-E

Dubochet, J., and N. Sartori Blanc. 2001. The cell in absence of aggregation artifacts. *Micron.* 32:91–99. doi:10.1016/S0968-4328(00)00026-3

Dubochet, J., M. Adrian, J.-J. Chang, J.-C. Homo, J. Lepault, A.W. McDowall, and P. Schultz. 1988. Cryo-electron microscopy of vitrified specimens. *Q. Rev. Biophys.* 21:129–228. doi:10.1017/S0033583500004297

Dulubova, I.L.X., X. Lou, J. Lu, I. Huryeva, A. Alam, R. Schneggenburger, T.C. Südhof, and J. Rizo. 2005. A Munc13/RIM/Rab3 tripartite complex: from priming to plasticity? *EMBO J.* 24:2839–2850. doi:10.1038/sj.emboj.7600753

Dunkley, P.R., J.W. Heath, S.M. Harrison, P.E. Jarvie, P.J. Glenfield, and J.A.P. Rostas. 1988. A rapid Percoll gradient procedure for isolation of synaptosomes directly from an S1 fraction: homogeneity and morphology of subcellular fractions. *Brain Res.* 441:59–71. doi:10.1016/0006-8993(88)91383-2

Fernández, J.-J., and S. Li. 2003. An improved algorithm for anisotropic nonlinear diffusion for denoising cryo-tomograms. *J. Struct. Biol.* 144:152–161. doi:10.1016/j.jsb.2003.09.010

Garvalov, B.K., B. Zuber, C. Bouchet-Marquis, M. Kudryashev, M. Gruska, M. Beck, A. Leis, F. Frischknecht, F. Bradke, W. Baumeister, et al. 2006. Luminal particles within cellular microtubules. *J. Cell Biol.* 174:759–765. doi:10.1083/jcb.200606074

Gerber, S.H., J.-C. Rah, S.-W. Min, X. Liu, H. de Wit, I. Dulubova, A.C. Meyer, J. Rizo, M. Arancillo, R.E. Hammer, et al. 2008. Conformational switch of syntaxin-1 controls synaptic vesicle fusion. *Science.* 321:1507–1510. doi:10.1126/science.1163174

Godino, Mdel.C., M. Torres, and J. Sánchez-Prieto. 2007. CB1 receptors diminish both $Ca^{(2+)}$ influx and glutamate release through two different mechanisms active in distinct populations of cerebrocortical nerve terminals. *J. Neurochem.* 101:1471–1482. doi:10.1111/j.1471-4159.2006.04422.x

Gotow, T., K. Miyaguchi, and P.H. Hashimoto. 1991. Cytoplasmic architecture of the axon terminal: filamentous strands specifically associated with synaptic vesicles. *Neuroscience.* 40:587–598. doi:10.1016/0306-4522(91)90143-C

Han, H.M., B. Zuber, and J. Dubochet. 2008. Compression and crevasses in vitreous sections under different cutting conditions. *J. Microsc.* 230:167–171. doi:10.1111/j.1365-2818.2008.01972.x

Harris, K.M., and P. Sultan. 1995. Variation in the number, location and size of synaptic vesicles provides an anatomical basis for the nonuniform probability of release at hippocampal CA1 synapses. *Neuropharmacology.* 34:1387–1395. doi:10.1016/0028-3908(95)00142-S

Harrison, S.M., P.E. Jarvie, and P.R. Dunkley. 1988. A rapid Percoll gradient procedure for isolation of synaptosomes directly from an S1 fraction: viability of subcellular fractions. *Brain Res.* 441:72–80. doi:10.1016/0006-8993(88)91384-4

Hirokawa, N., K. Sobue, K. Kanda, A. Harada, and H. Yorifuji. 1989. The cytoskeletal architecture of the presynaptic terminal and molecular structure of synapsin 1. *J. Cell Biol.* 108:111–126. doi:10.1083/jcb.108.1.111

Hosoi, N., M. Holt, and T. Sakaba. 2009. Calcium dependence of exo- and endocytotic coupling at a glutamatergic synapse. *Neuron.* 63:216–229. doi:10.1016/j.neuron.2009.06.010

Downloaded from http://rupress.org/jcb/article-pdf/188/1/145/1893572/jcb_200908082.pdf by guest on 08 February 2026

Janka, Z., and D.G. Jones. 1982. A morphometric study of cultured rat cerebral synapses exposed to different cationic media. *Brain Res.* 241:215–225. doi:10.1016/0006-8993(82)91058-7

Jovanovic, J.N., T.S. Sihra, A.C. Nairn, H.C. Hemmings Jr., P. Greengard, and A.J. Czernik. 2001. Opposing changes in phosphorylation of specific sites in synapsin I during Ca^{2+}-dependent glutamate release in isolated nerve terminals. *J. Neurosci.* 21:7944–7953.

Karatekin, E., V.S. Tran, S. Huet, I. Fanget, S. Cribier, and J.-P. Henry. 2008. A 20-nm step toward the cell membrane preceding exocytosis may correspond to docking of tethered granules. *Biophys. J.* 94:2891–2905. doi:10.1529/biophysj.107.116756

Kim, Y.-G., S. Raunser, C. Munger, J. Wagner, Y.-L. Song, M. Cygler, T. Walz, B.-H. Oh, and M. Sacher. 2006. The architecture of the multisubunit TRAPP I complex suggests a model for vesicle tethering. *Cell.* 127:817–830. doi:10.1016/j.cell.2006.09.029

Koss, D.J., K.P. Hindley, G. Riedel, and B. Platt. 2007. Modulation of hippocampal calcium signalling and plasticity by serine/threonine protein phosphatases. *J. Neurochem.* 102:1009–1023. doi:10.1111/j.1471-4159.2007.04579.x

Koster, A.J., R. Grimm, D. Typke, R. Hegerl, A. Stoschek, J. Walz, and W. Baumeister. 1997. Perspectives of molecular and cellular electron tomography. *J. Struct. Biol.* 120:276–308. doi:10.1006/jsbi.1997.3933

Kraszewski, K., L. Daniell, O. Mundigl, and P. De Camilli. 1996. Mobility of synaptic vesicles in nerve endings monitored by recovery from photobleaching of synaptic vesicle-associated fluorescence. *J. Neurosci.* 16:5905–5913.

Landis, D.M.D., A.K. Hall, L.A. Weinstein, and T.S. Reese. 1988. The organization of cytoplasm at the presynaptic active zone of a central nervous system synapse. *Neuron.* 1:201–209. doi:10.1016/0896-6273(88)90140-7

Lonart, G., S. Schoch, P.S. Kaeser, C.J. Larkin, T.C. Südhof, and D.J. Linden. 2003. Phosphorylation of RIM1α by PKA triggers presynaptic long-term potentiation at cerebellar parallel fiber synapses. *Cell.* 115:49–60. doi:10.1016/S0092-8674(03)00727-X

Lučić, V., F. Förster, and W. Baumeister. 2005a. Structural studies by electron tomography: from cells to molecules. *Annu. Rev. Biochem.* 74:833–865. doi:10.1146/annurev.biochem.73.011303.074112

Lučić, V., T. Yang, G. Schweikert, F. Förster, and W. Baumeister. 2005b. Morphological characterization of molecular complexes present in the synaptic cleft. *Structure.* 13:423–434. doi:10.1016/j.str.2005.02.005

Marks, B., and H.T. McMahon. 1998. Calcium triggers calcineurin-dependent synaptic vesicle recycling in mammalian nerve terminals. *Curr. Biol.* 8:740–749. doi:10.1016/S0960-9822(98)70297-0

Martens, S., and H.T. McMahon. 2008. Mechanisms of membrane fusion: disparate players and common principles. *Nat. Rev. Mol. Cell Biol.* 9:543–556. doi:10.1038/nrm2417

Masich, S., T. Ostberg, L. Norlén, O. Shupliakov, and B. Daneholt. 2006. A procedure to deposit fiducial markers on vitreous cryo-sections for cellular tomography. *J. Struct. Biol.* 156:461–468. doi:10.1016/j.jsb.2006.05.010

Maurer, U.E., B. Sodeik, and K. Grünewald. 2008. Native 3D intermediates of membrane fusion in herpes simplex virus 1 entry. *Proc. Natl. Acad. Sci. USA.* 105:10559–10564. doi:10.1073/pnas.0801674105

McMahon, H.T., P. Foran, J.O. Dolly, M. Verhage, V.M. Wiegant, and D.G. Nicholls. 1992. Tetanus toxin and botulinum toxins type A and B inhibit glutamate, gamma-aminobutyric acid, aspartate, and met-enkephalin release from synaptosomes. Clues to the locus of action. *J. Biol. Chem.* 267:21338–21343.

Medalia, O., M. Beck, M. Ecke, I. Weber, R. Neujahr, W. Baumeister, and G. Gerisch. 2007. Organization of actin networks in intact filopodia. *Curr. Biol.* 17:79–84. doi:10.1016/j.cub.2006.11.022

Nicholls, D.G., and T.S. Sihra. 1986. Synaptosomes possess an exocytotic pool of glutamate. *Nature.* 321:772–773. doi:10.1038/321772a0

Nickell, S., F. Förster, A. Linaroudis, W.D. Net, F. Beck, R. Hegerl, W. Baumeister, and J.M. Plitzko. 2005. TOM software toolbox: acquisition and analysis for electron tomography. *J. Struct. Biol.* 149:227–234. doi:10.1016/j.jsb.2004.10.006

Parpura, V., and U. Mohideen. 2008. Molecular form follows function: (un)snaring the SNAREs. *Trends Neurosci.* 31:435–443. doi:10.1016/j.tins.2008.06.003

Phillips, G.R., J.K. Huang, Y. Wang, H. Tanaka, L. Shapiro, W. Zhang, W.-S. Shan, K. Arndt, M. Frank, R.E. Gordon, et al. 2001. The presynaptic particle web: ultrastructure, composition, dissolution, and reconstitution. *Neuron.* 32:63–77. doi:10.1016/S0896-6273(01)00450-0

Rizzoli, S.O., and W.J. Betz. 2005. Synaptic vesicle pools. *Nat. Rev. Neurosci.* 6:57–69. doi:10.1038/nrn1583

Rosenmund, C., and C.F. Stevens. 1996. Definition of the readily releasable pool of vesicles at hippocampal synapses. *Neuron.* 16:1197–1207. doi:10.1016/S0896-6273(00)80146-4

Sankaranarayanan, S., P.P. Atluri, and T.A. Ryan. 2003. Actin has a molecular scaffolding, not propulsive, role in presynaptic function. *Nat. Neurosci.* 6:127–135. doi:10.1038/nn1002

Schiavo, G., M. Matteoli, and C. Montecucco. 2000. Neurotoxins affecting neuroexocytosis. *Physiol. Rev.* 80:717–766.

Schweizer, F.E., and T.A. Ryan. 2006. The synaptic vesicle: cycle of exocytosis and endocytosis. *Curr. Opin. Neurobiol.* 16:298–304. doi:10.1016/j.conb.2006.05.006

Shtrahman, M., C. Yeung, D.W. Nauen, G.Q. Bi, and X.L. Wu. 2005. Probing vesicle dynamics in single hippocampal synapses. *Biophys. J.* 89:3615–3627. doi:10.1529/biophysj.105.059295

Siksou, L., P. Rostaing, J.-P. Lechaire, T. Boudier, T. Ohtsuka, A. Fejtová, H.-T. Kao, P. Greengard, E.D. Gundelfinger, A. Triller, and S. Marty. 2007. Three-dimensional architecture of presynaptic terminal cytomatrix. *J. Neurosci.* 27:6868–6877. doi:10.1523/JNEUROSCI.1773-07.2007

Siksou, L., A. Triller, and S. Marty. 2009a. An emerging view of presynaptic structure from electron microscopic studies. *J. Neurochem.* 108:1336–1342. doi:10.1111/j.1471-4159.2009.05888.x

Siksou, L., F. Varoqueaux, O. Pascual, A. Triller, N. Brose, and S. Marty. 2009b. A common molecular basis for membrane docking and functional priming of synaptic vesicles. *Eur. J. Neurosci.* 30:49–56. doi:10.1111/j.1460-9568.2009.06811.x

Sim, A.T.R., H.G.E. Lloyd, P.E. Jarvie, M. Morrison, J.A.P. Rostas, and P.R. Dunkley. 1993. Synaptosomal amino acid release: effect of inhibiting protein phosphatases with okadaic acid. *Neurosci. Lett.* 160:181–184. doi:10.1016/0304-3940(93)90408-D

Soille, P. 2003. Morphological image analysis. Springer-Verlag, New York. 391 pp.

Stoppini, L., P.A. Buchs, and D. Muller. 1991. A simple method for organotypic cultures of nervous tissue. *J. Neurosci. Methods.* 37:173–182. doi:10.1016/0165-0270(91)90128-M

Südhof, T.C. 2004. The synaptic vesicle cycle. *Annu. Rev. Neurosci.* 27:509–547. doi:10.1146/annurev.neuro.26.041002.131412

Sztul, E., and V. Lupashin. 2006. Role of tethering factors in secretory membrane traffic. *Am. J. Physiol. Cell Physiol.* 290:C11–C26. doi:10.1152/ajpcell.00293.2005

Tripathi, A., Y. Ren, P.D. Jeffrey, and F.M. Hughson. 2009. Structural characterization of Tip20p and Dsl1p, subunits of the Dsl1p vesicle tethering complex. *Nat. Struct. Mol. Biol.* 16:114–123. doi:10.1038/nsmb.1548

Vaughan, R.A., R.A. Huff, G.R. Uhl, and M.J. Kuhar. 1997. Protein kinase C-mediated phosphorylation and functional regulation of dopamine transporters in striatal synaptosomes. *J. Biol. Chem.* 272:15541–15546. doi:10.1074/jbc.272.24.15541

Verhage, M., and J.B. Sørensen. 2008. Vesicle docking in regulated exocytosis. *Traffic.* 9:1414–1424. doi:10.1111/j.1600-0854.2008.00759.x

Wojcik, S.M., J.S. Rhee, E. Herzog, A. Sigler, R. Jahn, S. Takamori, N. Brose, and C. Rosenmund. 2004. An essential role for vesicular glutamate transporter 1 (VGLUT1) in postnatal development and control of quantal size. *Proc. Natl. Acad. Sci. USA.* 101:7158–7163. doi:10.1073/pnas.0401764101

Wu, X.-S., B.D. McNeil, J. Xu, J. Fan, L. Xue, E. Melicoff, R. Adachi, L. Bai, and L.-G. Wu. 2009. Ca(2+) and calmodulin initiate all forms of endocytosis during depolarization at a nerve terminal. *Nat. Neurosci.* 12:1003–1010. doi:10.1038/nn.2355

Zampighi, G.A., L.M. Zampighi, N. Fain, S. Lanzavecchia, S.A. Simon, and E.M. Wright. 2006. Conical electron tomography of a chemical synapse: vesicles docked to the active zone are hemi-fused. *Biophys. J.* 91:2910–2918. doi:10.1529/biophysj.106.084814

Zenisek, D., J.A. Steyer, and W. Almers. 2000. Transport, capture and exocytosis of single synaptic vesicles at active zones. *Nature.* 406:849–854. doi:10.1038/35022500

Zhou, Y., T.K. Frey, and J.J. Yang. 2009. Viral calciomics: interplays between Ca2+ and virus. *Cell Calcium.* 46:1–17. doi:10.1016/j.ceca.2009.05.005

Zuber, B., I. Nikonenko, P. Klauser, D. Muller, and J. Dubochet. 2005. The mammalian central nervous synaptic cleft contains a high density of periodically organized complexes. *Proc. Natl. Acad. Sci. USA.* 102:19192–19197. doi:10.1073/pnas.0509527102

Downloaded from http://rupress.org/jcb/article-pdf/188/1/145/1893572/jcb_200908082.pdf by guest on 08 February 2026